In-beam fast-timing measurements in ^{103,105,107}Cd

S. Kisyov,[1] S. Lalkovski,[1,*] N. Mărginean,[2] D. Bucurescu,[2] L. Atanasova,[3] D. L. Balabanski,[3] Gh. Căta-Danil,[2] I. Căta-Danil,[2] J.-M. Daugas,[4] D. Deleanu,[2] P. Detistov,[3] D. Filipescu,[2] G. Georgiev,[5] D. Ghiţă,[2] T. Glodariu,[2] J. Jolie,[6] D. S. Judson,[7] R. Lozeva,[5,8,9] R. Mărginean,[2] C. Mihai,[2] A. Negret,[2] S. Pascu,[2] D. Radulov,[1,†] J.-M. Régis,[6] M. Rudigier,[6] T. Sava,[2] L. Stroe,[2] G. Suliman,[2] N. V. Zamfir,[2] K. O. Zell,[6] and M. Zhekova[1]

[1]*Faculty of Physics, University of Sofia "St. Kliment Ohridski," BG-1164 Sofia, Bulgaria*
[2]*Horia Hulubei National Institute for Physics and Nuclear Engineering, RO-77125 Bucharest-Magurele, Romania*
[3]*Institute for Nuclear Research and Nuclear Energy, Bulgarian Academy of Science, BG-1784 Sofia, Bulgaria*
[4]*CEA, DAM, DIF, F-91297 Arpajon, France*
[5]*Centre de Spectrométrie Nucleaire et Spectrometrie de Masse, F-91405 Orsay-Campus, France*
[6]*Institut für Kernphysik, University of Cologne, D-50923 Cologne, Germany*
[7]*Department of Physics, University of Liverpool, Liverpool, United Kingdom*
[8]*Instituut voor Kern- en Stralingsfysica, Katholieke Universiteit Leuven, B-3001 Leuven, Belgium*
[9]*Institut Pluridisciplinaire Hubert Curien, Universit de Strasbourg, CNRS, IN2P3, F-67037 Strasbourg Cedex 2, France*

(Received 9 May 2011; revised manuscript received 13 June 2011; published 25 July 2011)

Fast-timing measurements were performed in the region of the medium-mass ^{103,105,107}Cd isotopes, produced in fusion evaporation reactions. Results on new and reevaluated half-lives are analyzed within a systematic study of transition rates. The $7/2^+_1$ states in ^{103,105,107}Cd are interpreted as arising from a single-particle excitation. The $9/2^+$ states configuration assignment is based on the observed decay branches.

DOI: 10.1103/PhysRevC.84.014324 PACS number(s): 21.10.Hw, 21.10.Tg, 23.20.Lv, 27.60.+j

I. INTRODUCTION

Cadmium isotopes have two protons less than the $_{50}$Sn nuclei, presenting a good test case for the robustness of the shell structure. Shell-model calculations successfully describe the experimentally observed level energies and level lifetimes in the extreme neutron-rich and neutron-deficient cadmium isotopes, proving the persistence of the shell structure below the doubly magic ^{132}Sn and ^{100}Sn nuclei [1–4]. Fingerprints of collectivity, however, start to emerge when moving away from the neutron shell closures. They can be found in the decrease of the 2^+_1 energy and in the increase of the respective $B(E2; 2^+_1 \rightarrow 0^+_1)$ values when approaching the neutron mid shell [5].

Due to the neighborhood of the shell-model tin isotopes and the presence of weak collectivity in the neutron–mid-shell cadmium isotopes, both single-particle and collective states are expected to occur in the medium-mass odd-A Cd nuclei. Moreover, there are several cases where the structure of the state is ambiguous. In the ^{103,105,107}Cd [6–8], for example, the lowest-lying excited $J^\pi = 7/2^+$ state can arise from a collective excitation built on the $5/2^+$ ground state or from a single-particle excitation. A model-independent approach to the problem is to evaluate the $B(E2)$ transition strengths within a systematic study involving even-even well-deformed and spherical nuclei, where the structure is well established.

In order to study the structure of the low-lying excited states in ^{103,105,107}Cd, fast-timing measurements were performed. The half-lives are directly related to the transition rates and hence to the structure of the state.

II. EXPERIMENTAL SETUP

The low-lying excited states, placed on and close to the yrast line in ^{103}Cd, ^{105}Cd, and ^{107}Cd, were populated via fusion evaporation reactions. A carbon beam, accelerated to 50 MeV by the tandem accelerator of the National Institute for Physics and Nuclear Engineering in Magurele, Romania, was impinged on self-supporting 10-mg/cm^2-thick ^{94,96}Mo targets and on a 1-mg/cm^2-thick ^{98}Mo target with 20-μm Pb backing. The three targets were isotopically enriched up to 98.97% in ^{94}Mo, 95.70% in ^{96}Mo, and 98% in ^{98}Mo, respectively.

The cross section for the ^{94}Mo(^{12}C,3n)^{103}Cd reaction was calculated to be 100 mb, while for the ^{96}Mo(^{12}C,3n)^{105}Cd and ^{98}Mo(^{12}C,3n)^{107}Cd reactions, it was approximately 400 mb. The typical beam intensity was of the order of 8 pnA. Besides the 3n channels, the 4n, 2np, 4np, and 2$n\alpha$ fusion evaporation channels also have significant cross sections, which contaminate the spectra of interest.

The half-lives of the levels of interest were deduced by using a fast-timing setup consisting of five $LaBr_3$:Ce scintillator detectors working in coincidence with eight HPGe detectors [9]. Five of the HPGe detectors were placed at backward angles with respect to the beam axis, two were placed at 90°, and the eighth HPGe detector was placed at a forward angle. The five $LaBr_3$:Ce detectors were mounted below the target chamber on a ring of approximately 45° with respect to the beam axis. The detectors were equipped with crystals of cylindrical shape that had 5% Ce doping. One of the $LaBr_3$:Ce detectors was a commercial integral detector, equipped with a 2×2 in. crystal. Two of the noncommercial $LaBr_3$:Ce detectors had crystals with size of 1 in. in height and a diameter of 1 in. Two of the noncommercial $LaBr_3$:Ce detectors was comprised of 1.5×1.5 in. crystals. Each of the four crystals was optically coupled to an XP20D0B photomultiplier tube and mounted

*stl@phys.uni-sofia.bg
†Present address: Katholieke Universiteit, Leuven, Belgium.

in an aluminum casing. The readout from each of the four noncommercial detectors was made via a VD184/T voltage divider. The voltage dividers from the commercial and the noncommercial detectors issued a negative anode signal and a fast positive dynode signal. The anode signal was used for timing, while the dynode signal was used to obtain energy information. This nonconventional choice was made to avoid the saturation of the dynode signal [9], which facilitates the analysis of the energy spectra.

The energy signals from the HPGe detectors were amplified and then digitized by 8-k analog-to-digital converters (ADCs) AD413A. The timing signals from the HPGe detectors were processed by 4-k 4418/T time-to-digital converters. The energy signals from the $LaBr_3$:Ce detectors were amplified by spectroscopic amplifiers and then digitized by 8-k ADCs AD413A. The timing signals from the $LaBr_3$:Ce detectors were sent to a quad constant fraction discriminator (CFD) (model 935). Each of the five timing signals was used to start a time-to-amplitude converter (TAC) operating in a common stop mode. Then the five TAC output signals were sent to 8-k ADCs. The acquisition was triggered when two $LaBr_3$:Ce and one HPGe detectors were fired in coincidence. The absolute photopeak efficiency, measured with a ^{137}Cs source, was 0.8% for the $LaBr_3$:Ce part and 1.5% for the HPGe part of the detector array.

III. DATA ANALYSIS

The data were stored in event-by-event mode in 100-MB long files, which were grouped in runs of approximately two hours. Then the data were analyzed using the GASPWARE and RADWARE [10] packages. Because of the instability of the $LaBr_3$:Ce detectors observed with time, a gain-matching procedure was applied run by run. To correct the CFD for the walk effect, which was observed at low energies, an analysis of the time response as a function of energy was performed with a ^{60}Co source [9] and in-beam. Then the data were sorted in gated energy spectra, two-dimensional energy-energy (E_γ–E_γ) and three-dimensional energy-energy-time (E_γ–E_γ–ΔT) matrices, where E_γ is the γ-ray energy detected by a $LaBr_3$:Ce detector and ΔT is a time difference between two γ rays detected in coincidence.

The (E_γ–E_γ–ΔT) matrices were constructed as fully symmetric in energy, i.e., for each event where γ rays of energies $E_{\gamma 1}$ and $E_{\gamma 2}$ are detected, the matrix elements ($E_{\gamma 1}$, $E_{\gamma 2}$) and ($E_{\gamma 2}$, $E_{\gamma 1}$) are incremented, while the time intervals associated with these two points are calculated as $\Delta T = (t_1 - t_2) + t_0$ and $\Delta T = -(t_1 - t_2) + t_0$, respectively. Here, $t_1 - t_2 > 0$ is the time difference measured with two TACs, and t_0 is an arbitrary offset. In the cases where the two γ rays feed and de-excite a state with a half-life longer than the electronics resolution, which in the present work is 6 ps/channel, the time distributions associated with the two matrix elements ($E_{\gamma 1}$, $E_{\gamma 2}$) and ($E_{\gamma 2}$, $E_{\gamma 1}$) will be shifted by 2τ, where τ is the lifetime of the level of interest. This procedure represents the centroid shift method [11], which has been successfully used in the past [12] and recently applied with $LaBr_3$:Ce detectors [9]. In the cases where the level half-life is much longer than the detector time resolution, an exponential tail emerges and the slope method has been used to determine the half-life of the level. Deconvolution of the Gaussian and exponent was applied in the cases where the half-life of the level is of the order of the full width at half maximum (FWHM) of the prompt distribution.

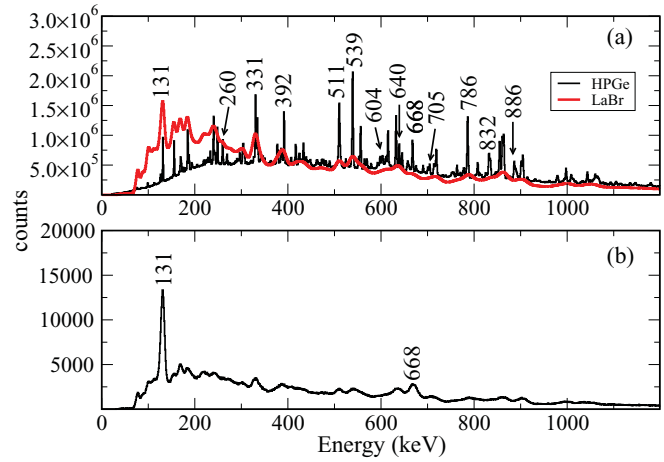

FIG. 1. (Color online) ^{105}Cd energy spectra: (a) Total projection from all HPGe and $LaBr_3$:Ce detectors; (b) $LaBr_3$:Ce energy spectrum gated on a 886-keV transition in any of the HPGe detectors. The labels denote transitions in ^{105}Cd.

In order to select a particular reaction channel and particular γ-decay branch leading to the state of interest, the matrices were constructed with a condition imposed on prompt γ rays detected in any of the high-resolution HPGe detectors.

Figure 1(a) shows the energy total projection for the ^{12}C+^{96}Mo→^{105}Cd+3n reaction for all HPGe and $LaBr_3$:Ce detectors. At low energies, the higher efficiency of the $LaBr_3$:Ce with respect to the HPGe detectors is remarkable. The energies of ^{105}Cd are marked with numbers. Figure 1(b) represents the $LaBr_3$:Ce energy spectrum, gated on the 886-keV transition from ^{105}Cd in the HPGe detectors, which improves the peak-to-background ratio. Similar spectra were constructed for the other two reactions, ^{12}C+^{94}Mo→^{103}Cd+3n and ^{12}C+^{98}Mo→^{107}Cd+3n.

Figure 2 presents time spectra obtained after two-dimensional energy gates were imposed on E_γ–E_γ–ΔT matrices, which were gated on prompt transitions with HPGe detectors. To increase the statistics, in each of the cases, several prompt gates were imposed on the HPGe detectors. Here, the procedure will be illustrated by using the lowest-lying prompt and delayed transitions (Fig. 3), as seen in the present work.

Figure 2(a) presents the time distributions for the decay of the $7/2_1^+$ state in ^{107}Cd (Fig. 3). The time distribution, which is plotted in solid lines, is obtained with a (205γ, 641γ) energy gate, imposed on the $LaBr_3$:Ce detectors, while the symmetric (641γ, 205γ) gate is plotted with dots. The half-life of 0.68(4) ns, obtained from the centroid shift method, is consistent with the NNDC value of $T_{1/2}$ =0.71(4) ns [8]. Gates on 798-keV or 956-keV transitions were applied with HPGe detectors in order to clean the time spectra from background events.

Figure 2(b) presents the time curves for the decay of the $7/2_1^+$ state in ^{105}Cd (Fig. 3). The half-life of 1.66(12) ns,

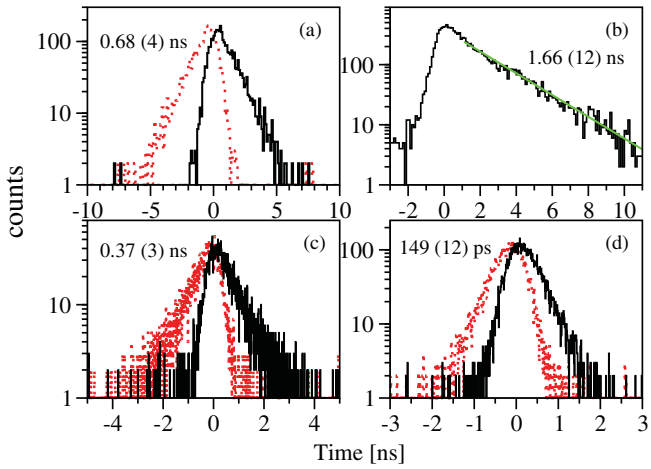

FIG. 2. (Color online) Time spectra obtained for the decay of the $7/2_1^+$ states in (a) ^{107}Cd, (b) ^{105}Cd, (c) ^{103}Cd, and (d) for the $11/2_1^-$ state in ^{105}Cd. Time distributions, plotted with solid lines, are gated on ($E_{\gamma 1}$, $E_{\gamma 2}$), while the dotted lines describe the symmetric time distribution gated on ($E_{\gamma 2}$, $E_{\gamma 1}$) (for more details see the text).

obtained in the present study, was measured from the slope of the time distribution gated on (668γ,131γ) with the $LaBr_3$:Ce detectors and cleaned with a gate on the 886-keV γ ray or 705-keV γ ray imposed on any of the eight HPGe detectors. The half-life, measured in the present study, is consistent with the $T_{1/2}$ =1.75(11) ns, which is based on a $\gamma(t)$ measurement with one NaI(Tl) detector [13] and adopted by NNDC [7].

Figure 2(c) presents the time curves for the decay of the $7/2_1^+$ state in ^{103}Cd (Fig. 3). The half-life of 0.37(3) ns was obtained from the centroid shift of the two time distributions generated with gates on the 188-keV and 720-keV transitions, imposed on any two of the $LaBr_3$:Ce detectors in coincidence with the 921-keV or 623-keV γ rays detected in any of the HPGe detectors.

The half-life of the $11/2_1^-$ state [Fig. 2(d)] in ^{105}Cd (Fig. 3) was obtained by gating on the 539-keV and 392-keV transitions, detected by any two of the five $LaBr_3$:Ce detectors. An additional gate on the 786-keV γ ray, which is in coincidence with the 392-keV and 539-keV transitions (Fig. 3), was imposed on any of the HPGe detectors. The half-life, deduced from the centroid shift of the two mirror time spectra, is 149(12) ps.

IV. DISCUSSION

A. $7/2_1^+$

The $7/2_1^+$ level energies E_i and half-lives $T_{1/2}$ for ^{103,105,107}Cd nuclei [6–8] are listed in Table I, along with the γ-ray energies E_γ, multipolarities $L\lambda$, and mixing ratios δ of the de-exciting transitions. The $J^\pi = 7/2^+$ state is the first excited state in all three isotopes and decays via an $M1$+$E2$ transition to the ground state. An upper limit of the mixing ratio $\delta \leqslant 0.1$ for the $7/2_1^+ \rightarrow 5/2_1^+$ transition in ^{103}Cd has been estimated by the NNDC [6]. The mixing ratio, adopted for the $M1$+$E2$ transition in ^{107}Cd, is $\delta = +0.25(1)$ [8]. It has been suggested that the respective transition in ^{105}Cd is of an almost pure $M1$ nature, however, a small $E2$ admixture is assumed [7]. For the purpose of the current discussion, an upper limit of $\delta \leqslant 0.1$ was adopted in the present study.

The reduced transition probabilities, calculated with RULER [5], are given in the last column of Table I.

Figure 4 shows the systematic trend of the $B(M1)$ [Fig. 4(a)] and $B(E2)$ values for the $7/2_1^+ \rightarrow 5/2_1^+$ transitions in $^{103-111}Cd_{55-63}$ [Fig. 4(b)], compared to the $B(E2; 2_1^+ \rightarrow 0_1^+)$ for their even-even Cd cores. Figure 5 shows the evolution of

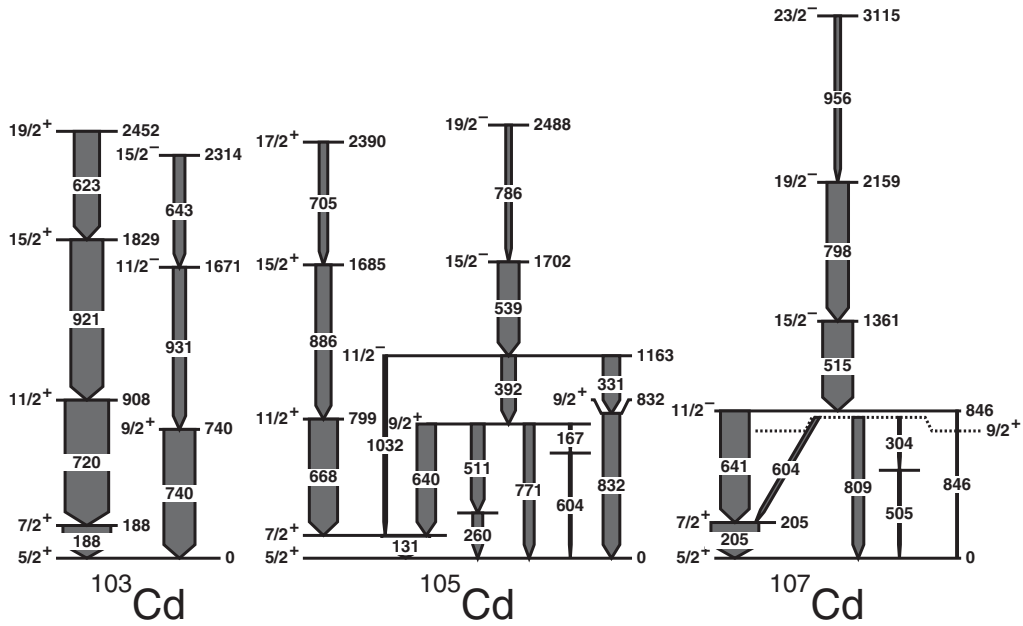

FIG. 3. Partial level schemes of ^{103,105,107}Cd.

TABLE I. First excited $7/2^+$ state in ^{103,105,107}Cd and decay properties.

Isotope	E_i (keV)	$T_{1/2}$	E_γ (keV)	$L\lambda$	δ	$B(\lambda L)$ (W.u.)
^{103}Cd	188	0.37(3) ns	188	M1	$\leqslant 0.1$	0.0089(8)
				E2		2.27(19)
^{105}Cd	131	1.66(12) ns	131	M1	$\leqslant 0.1$	0.0058(5)
				E2		2.93(22)
^{107}Cd	205	0.68(4) ns	205	M1	0.25(1)	0.00331(20)
				E2		4.2(4)

the $B(E2; 2_1^+ \rightarrow 0_1^+)$ transition rates with the neutron number for all even-even nuclei in the $40 \leqslant Z \leqslant 50$ region.

In the $^{103-107}Cd_{55-59}$ nuclei, because of the low mixing ratio, the $B(E2; 7/2_1^+ \rightarrow 5/2_1^+)$ transition strengths are significantly suppressed in comparison to the $B(E2; 2_1^+ \rightarrow 0_1^+)$ values for the even-even Cd cores [Fig. 4(b)]. Moreover, they are two orders of magnitude weaker than the $B(E2; 2_1^+ \rightarrow 0_1^+)$ values for the most deformed neutron mid-shell Zr and Mo nuclei (Fig. 5). In fact, the ^{103,105,107}Cd $B(E2; 7/2_1^+ \rightarrow 5/2_1^+)$ values are similar to the reduced transition probabilities for the magic tin nuclei (Fig. 5), suggesting a single-particle nature of the $7/2_1^+$ state, most probably arising from the $\nu g_{7/2}$ configuration.

In $^{109}Cd_{61}$, the $7/2_1^+$ state appears 203 keV above the $5/2^+$ ground state and decays, according to NNDC, via a pure M1 transition giving rise to $B(M1)$(W.u.) = 0.068(12) [14], which is an order of magnitude higher than the respective value in $^{103-107}$Cd. However, the odd behavior of the $B(M1)$ point on Fig. 4 suggests a significant $E2$ component. In fact, such an increase of the $B(E2)$ value, and hence in the collectivity of the state, is observed in ^{111}Cd. There, the $5/2_1^+$ and $7/2_1^+$ states appear at 245 and 416 keV, respectively [15]. The $7/2_1^+$ state has a half-life of 0.12 ns and decays to the $5/2_1^+$ state via a 171-keV $M1+E2$ transition. The mixing ratio $\delta = -0.144$ of this transition leads to $B(E2; 7/2_1^+ \rightarrow 5/2_1^+) = 23(6)$ W.u., which approaches the $B(E2; 2_1^+ \rightarrow 0_1^+)$ value in the even-even

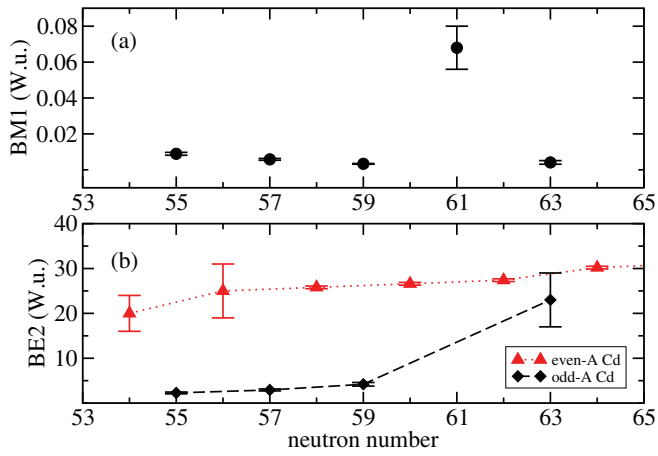

FIG. 4. (Color online) Systematics of (a) $B(M1; 7/2_1^+ \rightarrow 5/2_1^+)$ values for odd-A cadmium nuclei and (b) $B(E2; 7/2_1^+ \rightarrow 5/2_1^+)$ values for odd-A cadmium isotopes (diamonds) compared to the $B(E2; 2_1^+ \rightarrow 0_1^+)$ values in even-even cadmium cores (triangles).

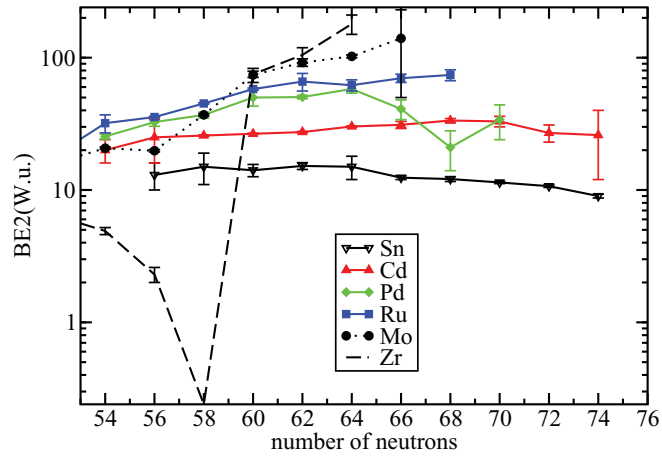

FIG. 5. (Color online) Systematics of $B(E2; 2_1^+ \rightarrow 0_1^+)$ transition rates for the even-even nuclei with $40 \leqslant Z \leqslant 50$.

cadmium cores [Fig. 4(b)], and hence the $7/2_1^+$ state becomes collective.

B. $11/2_1^-$

The $J^\pi = 11/2_1^-$ level appears in all odd-A cadmium isotopes from ^{103}Cd to ^{125}Cd [5]. It is observed at 1671 keV in ^{103}Cd and decreases in energy when approaching the neutron mid shell. In ^{117}Cd, it is placed 136 keV above the ground state. Further, the $11/2_1^-$ energy increases with the neutron number and, in ^{123}Cd, it is placed 317 keV above the ground state.

In $^{103-107}$Cd, the energy gap between the $11/2_1^-$ state and the ground state is larger than in the heavier cadmium nuclei, opening space for several states of single-particle and collective nature to appear. In $^{103-107}$Cd, the level decays via low-multipolarity transitions, where the $E1$ branch is dominant. In ^{109}Cd and ^{111}Cd, the state decays via $M2$ and $E3$ transitions, respectively, while in ^{113}Cd, a weak $E5$ γ branch is observed. Due to the level energy decrease and the γ-ray multipolarity increase with the mass number, the level half-life increases from 71 ns at ^{107}Cd to 14.1 y in ^{113}Cd. In $^{113-125}$Cd, the $11/2_1^-$ isomer decays to the respective indium isobars via β-decay. The half-life of the level decreases again with the mass number to 0.48 s at ^{125}Cd.

The half-life analysis, performed in the present work, along with the previously measured half-life of the $11/2_1^-$ state in ^{107}Cd, allows a systematic study of the $E1$ transition strengths, and hence the structure of the final $9/2^+$ state in a number of odd-A cadmium nuclei. In ^{107}Cd, the $11/2_1^-$ level decays via a branch of 37γ $E1$, 641γ $M2$, and 846γ $E3$ transitions, with $B(E1; 11/2^- \rightarrow 9/2^+) = 6.6 \times 10^{-6}(12)$ W.u., $B(M2; 11/2^- \rightarrow 7/2^+) = 0.123(10)$ W.u., and $B(E3; 11/2^- \rightarrow 5/2^+) = 1.3(4)$ W.u. [5], respectively.

The $11/2_1^-$ state in ^{105}Cd decays via 331-keV $E1$, 392-keV $E1$, and 1032-keV $M2$ transitions (Fig. 3). The γ-ray intensity ratio $I_{331\gamma} : I_{392\gamma} : I_{1032\gamma} = 100 : 82 : 79$ was adopted in [7]. The present study confirms the $I_{331\gamma} : I_{392\gamma}$ intensity ratio, however, the 1032-keV $M2$ transition was observed with $I_{331\gamma} : I_{1032\gamma} = 100 : 6$. Given the half-life of the level is $T_{1/2} = 149$ ps and the intensity ratio observed in the present work, the $M2$ transition strength is evaluated

to $B(M2;\ 11/2^- \rightarrow 7/2^+) = 0.254(21)$ W.u., while $B(E1;\ 11/2^- \rightarrow 9/2^+) = 3.0 \times 10^{-5}(3)$ W.u. and $B(E1;\ 11/2^- \rightarrow 9/2^+) = 1.47 \times 10^{-5}(14)$ W.u. for the 331-keV and 392-keV transitions, respectively.

The $11/2^-$ level in ^{103}Cd decays via a 931-keV $E1$ transition to a $9/2^+$ level (Fig. 3). No time structure of the decaying transition was observed in the present work. Therefore, an upper limit of 6 ps was deduced for the half-life of the level, leading to a $B(E1;\ 11/2^- \rightarrow 9/2^+) > 6.3 \times 10^{-5}$ W.u.

The systematic analysis shows that in $^{103-107}$Cd, the $9/2^+$ levels are fed by $E1$ transitions of similar strengths, suggesting a similar structure of the final state. Also, given the $9/2^+$ states decay to the $5/2^+_1$ ground states via prompt $E2$ transitions, a significant $5/2^+_1 \otimes 2^+_1$ component of the wave function is expected to occur at $9/2^+$.

V. CONCLUSION

Excited states in ^{103,105,107}Cd have been populated via fusion evaporation reactions. Half-lives of several excited states were measured by using the delayed coincidence technique. The half-life of the $7/2^+_1$ state in ^{107}Cd and ^{105}Cd was confirmed. The half-life of the first excited state in ^{103}Cd and of the $11/2^-_1$ in ^{105}Cd are newly obtained, allowing a systematic study of the transition strengths. The $B(E2;\ 7/2^+_1 \rightarrow 5/2^+_1)$ transition strengths in $^{103-107}$Cd are strongly hindered with respect to the $B(E2;\ 2^+_1 \rightarrow 0^+_1)$ values, observed in the most deformed nuclei in the region, suggesting a single-particle nature for the $7/2^+_1$ states. The $9/2^+$ states in ^{103,105,107}Cd are interpreted as arising from a $5/2^+_1 \otimes 2^+_1$ configuration.

ACKNOWLEDGMENTS

The work is supported by the Bulgarian Science Fund under Contracts No. DMU02/1, No. DRNF02/5, and No. DID-05/16; by the National Authority of the Scientific Research of Romania under Contracts No. PN09 37 01 05 and No. 24EU-ISOLDE/13.04.2009; and by Bulgarian-Romanian partnership Contracts No. BRS-07/23 and No. 460/PNII Module III.

[1] A. Jungclaus *et al.*, Phys. Rev. Lett. **99**, 132501 (2007).
[2] L. Caceres *et al.*, Phys. Rev. C **79**, 011301 (2009).
[3] F. Naqvi *et al.*, Phys. Rev. C **82**, 034323 (2010).
[4] A. Blazhev *et al.*, Phys. Rev. C **69**, 064304 (2004).
[5] NNDC data base [http://www.nndc.bnl.gov/ensdf/].
[6] D. de Frenne, Nucl. Data Sheets **110**, 2081 (2009).
[7] D. de Frenne and E. Jacobs, Nucl. Data Sheets **105**, 775 (2005).
[8] J. Blachot, Nucl. Data Sheets **109**, 1383 (2008).
[9] N. Mărginean *et al.*, Eur. Phys. J. A **46**, 329 (2010).
[10] D. Radford, Nucl. Instrum. Meth. A **361**, 297 (1995).
[11] W. Andrejtscheff, M. Senba, N. Tsoupas, and Z. Z. Ding, Nucl. Instrum. Meth. **204**, 123 (1982).
[12] W. Andrejtscheff, L. K. Kostov, H. Rotter, H. Prade, F. Stary, M. Senba, N. Tsoupas, Z. Z. Ding, and P. Raghavan, Nucl. Phys. A **437**, 167 (1985).
[13] R. Rougny, M. Meyer-Lévy, R. Béraud, J. Rivier, and R. Moret, Phys. Rev. C **8**, 2332 (1973).
[14] J. Blachot, Nucl. Data Sheets **107**, 355 (2006).
[15] J. Blachot, Nucl. Data Sheets **110**, 1239 (2009).